Heliyon

Received:
7 May 2016
Revised:
21 June 2016
Accepted:
15 July 2016

Heliyon 2 (2016) e00133

A small molecule-based strategy for endothelial differentiation and three-dimensional morphogenesis from human embryonic stem cells

Yijie Geng*, Bradley Feng

Department of Cell and Developmental Biology, University of Illinois at Urbana–Champaign, Urbana, IL 61801, USA

*Corresponding author. Department of Cell and Developmental Biology, University of Illinois at Urbana–Champaign, 601 S. Goodwin Ave., Urbana, IL 61801, USA.
E-mail address: geng2@illinois.edu (Y. Geng).

Abstract

The emerging models of human embryonic stem cell (hESC) self-organizing organoids provide a valuable *in vitro* platform for studying self-organizing processes that presumably mimic *in vivo* human developmental events. Here we report that through a chemical screen, we identified two novel and structurally similar small molecules BIR1 and BIR2 which robustly induced the self-organization of a balloon-shaped three-dimensional structure when applied to two-dimensional adherent hESC cultures in the absence of growth factors. Gene expression analyses and functional assays demonstrated an endothelial identity of this balloon-like structure, while cell surface marker analyses revealed a VE-cadherin^{+}CD31^{+}CD34^{+}KDR^{+}CD43^{-} putative endothelial progenitor population. Furthermore, molecular marker labeling and morphological examinations characterized several other distinct DiI-Ac-LDL^{+} multi-cellular modules and a VEGFR3^{+} sprouting structure in the balloon cultures that likely represented intermediate structures of balloon-formation.

http://dx.doi.org/10.1016/j.heliyon.2016.e00133

Keywords: Developmental biology, Cell biology

1. Introduction

The molecular and cellular mechanisms of organogenesis remain a key question of developmental biology. Self-organizing organoids derived from hESCs represent an attractive model platform for studying human organogenesis *in vitro*. Yoshiki Sasai's group pioneered this field by developing a series of culture conditions that induced hESCs to undergo differentiation programs that mimicked various aspects of early human neurogenesis [1, 2, 3, 4, 5, 6]. Several groups later developed their own approaches for organoid-formation [7, 8, 9, 10, 11, 12, 13, 14]. While all these studies adopted a suspension culture system, a different approach was developed for the self-organization of intestine-like [15, 16, 17] and kidney-like [18] organoids, in which three-dimensional (3-D) organoids were induced to grow out of two-dimensional (2-D) adherent cultures.

A delicate state of balance exists between the pluripotency regulatory network and the differentiation regulatory pathways, and is required for the maintenance of pluripotency [19, 20]. Disrupting this balanced state, by altering the expressions or activities of different components important for the maintenance of this balance, will trigger differentiation in different ways and toward different directions; for example, inhibition of heat shock 70 kDa protein 8 (HSPA8) by a small molecule leads to un-directional differentiation [21], whereas small molecule inhibition of TRPM6/TRPM7 magnesium channel activity specifically enhances mesoderm and definitive endoderm differentiations [22]. We thus hypothesized that by applying a stimulus that undermines this delicate balance in a certain way during the initial phase of differentiation, hESCs may be poised to differentiate in such a way that a self-organizing organoid structure can be generated. Because small molecules provide a source of practically inexhaustible structural diversity, we proposed to test this hypothesis by searching for small molecule inducers of organoid-formation through a chemical screen.

Here we report the identification of two novel small molecules, hereafter referred to as Balloon Inducing Reagent (BIR) 1 and 2, which triggered a spontaneous self-organizing program that led to the formation of a 3-D balloon-shaped structure during hESC differentiation. Using gene expression analyses, functional assays, and cell surface marker expression analysis, we demonstrated an endothelial identity of the balloons, and identified a putative endothelial progenitor population with a characteristic surface marker expression profile of VE-cadherin^{+}CD31^{+}CD34^{+}KDR^{+}CD43^{-}. We further studied the spontaneous emergence of a series of DiI-Ac-LDL^{+} multi-cellular modules in the balloon cultures which we believe may represent intermediate structures of balloon formation.

http://dx.doi.org/10.1016/j.heliyon.2016.e00133

2. Results

2.1. Morphological screen identified two structurally similar compounds that induced a self-organizing balloon-like structure

We previously conducted a high throughput chemical screen which identified 29 bioactive small molecules that potently disrupted hESC pluripotency [21]. Using this compound collection, we conducted a small-scale morphological screen (Fig. 1A and Methods and Materials) to search for small molecules capable of inducing self-organization of 3-D organoid structures. Briefly, hESCs were seeded as 2-D adherent cultures in order to allow the emergence of 3-D organoid-like structures to be readily identifiable. The screen consisted of two consecutive

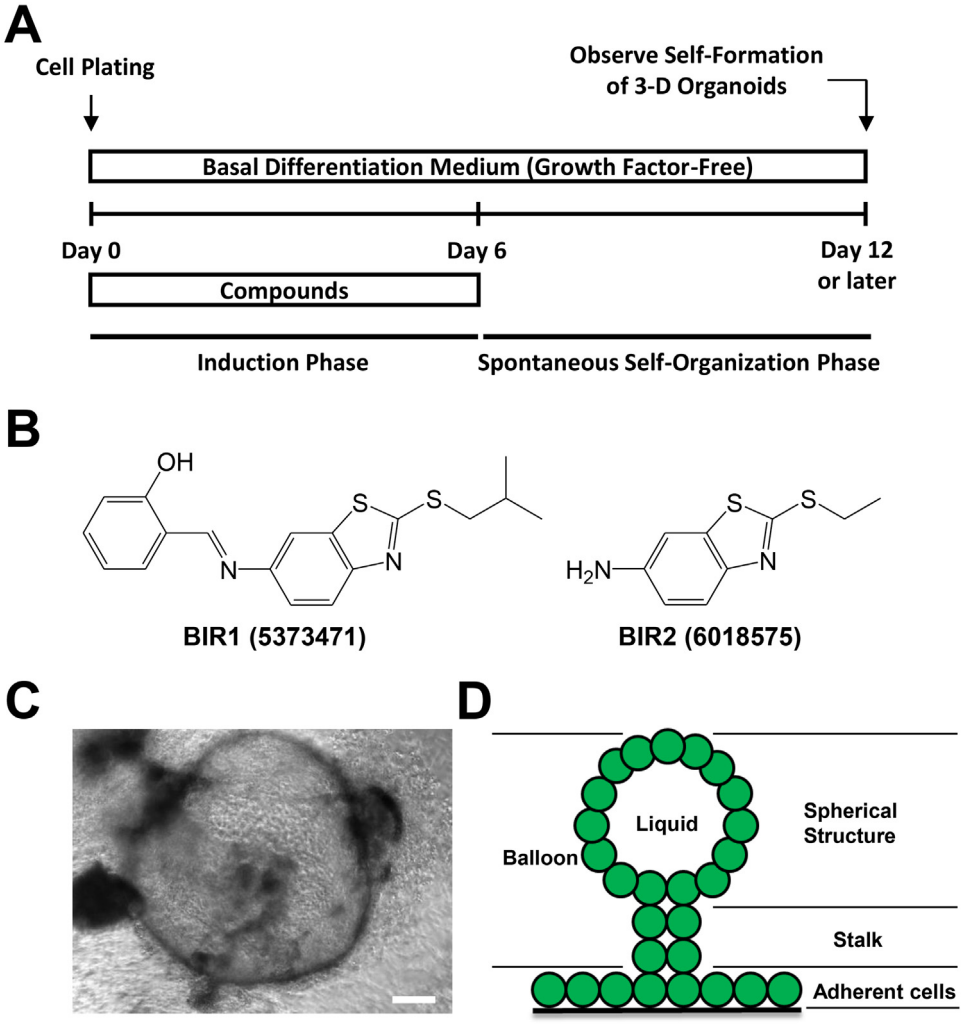

Fig. 1. Morphological screening identified compounds 5373471 (BIR1) and 6018575 (BIR2) as inducers of a self-organizing balloon-shaped structure. (A) Schematic overview of the morphological screening. (B) Chemical structures of 5373471 (BIR1) and 6018575 (BIR2). (C) Phase contrast image of a balloon structure. Scale bar: 200 μm. (D) Schematic drawing of a typical balloon.

http://dx.doi.org/10.1016/j.heliyon.2016.e00133

phases: in the "induction phase", small molecules were applied to hESCs for 6 days, a period long enough to induce differentiation; this is followed by the "spontaneous self-organization phase" during which small molecules were withdrawn, and cultures were let-grow in a basal differentiation medium in the absence of small molecules for a prolonged period of time. Cultures were monitored regularly starting from day 12 of differentiation induction for the spontaneous emergence of 3-D organoid-like structures. Both phases were growth factor-free.

From this screen we identified two structurally similar compounds 5373471 and 6018575 (Fig. 1B; ChemBridge) which, when individually applied to hESC cultures, each induced the formation of a self-organizing balloon-shaped structure (Fig. 1C; hereafter referred to as "balloons"). We thus named these molecules Balloon Inducing Reagent (BIR) 1 [5373471] and 2 [6018575], respectively. For a typical balloon induction process, hESCs were incubated with BIR1 (5 μM) or BIR2 (5 μM) for 6 days (day 0 to day 6) in a 2-D adherent culture system, and then let-grow in the absence of BIRs. Balloon structures generally emerged on days 12–13 at a density of approximately 1 balloon/cm^2. Specifically, BIR1 treatment gave rise to an average balloon density of 1.2 ± 0.8 balloons/cm^2 (mean ± SD; n = 4 independent experiments), while BIR2 treatment gave rise to an average density of 1.1 ± 0.1 balloons/cm^2 (mean ± SD; n = 3 independent experiments). According to the statistics, BIR1 treatments produced a higher level of variations in balloon density (±0.8 compared to ±0.1 for BIR2), which was in line with our general observation that although BIR1 and BIR2 gave rise to comparable average numbers of balloons (1.2 versus 1.1 balloons/cm^2), BIR2 tended to perform more consistently between different batches of experiments. We have also tested 1 μM, 2.5 μM, and 10 μM concentrations for both compounds: neither compound induced balloon formation at 1 μM; BIR1, but not BIR2, was able to induce balloon formation at 2.5 μM; at 10 μM, both BIR1 and BIR2 appeared to be toxic to the cells, and were unable to induce balloon formation.

A schematic drawing of a typical balloon structure is shown in Fig. 1D. A balloon typically consisted of two parts: a closed spherical structure suspended in culture medium and a stalk-shaped structure ("stalks" hereafter) with varying lengths linking the suspended spherical structure to adherent cells (Fig. 1C). The spherical structures were always filled with colorless fluid, and continued to accumulate fluid and bulge during prolonged periods of culture. A series of z-stack images from the bottom to the top (1 to 5) of a balloon are shown in Fig. 2A, demonstrating the stalk structure (1; white dashed circle), the connection between the tip of the stalk and the bottom of the spherical structure (2 and 3; white dashed circles), and body of the spherical structure (4 and 5; focusing on the wall of the spherical structure, white arrows). A diameter of around 0.5 mm was commonly seen for spherical structures; the largest of these structures could grow to > 1 mm

http://dx.doi.org/10.1016/j.heliyon.2016.e00133

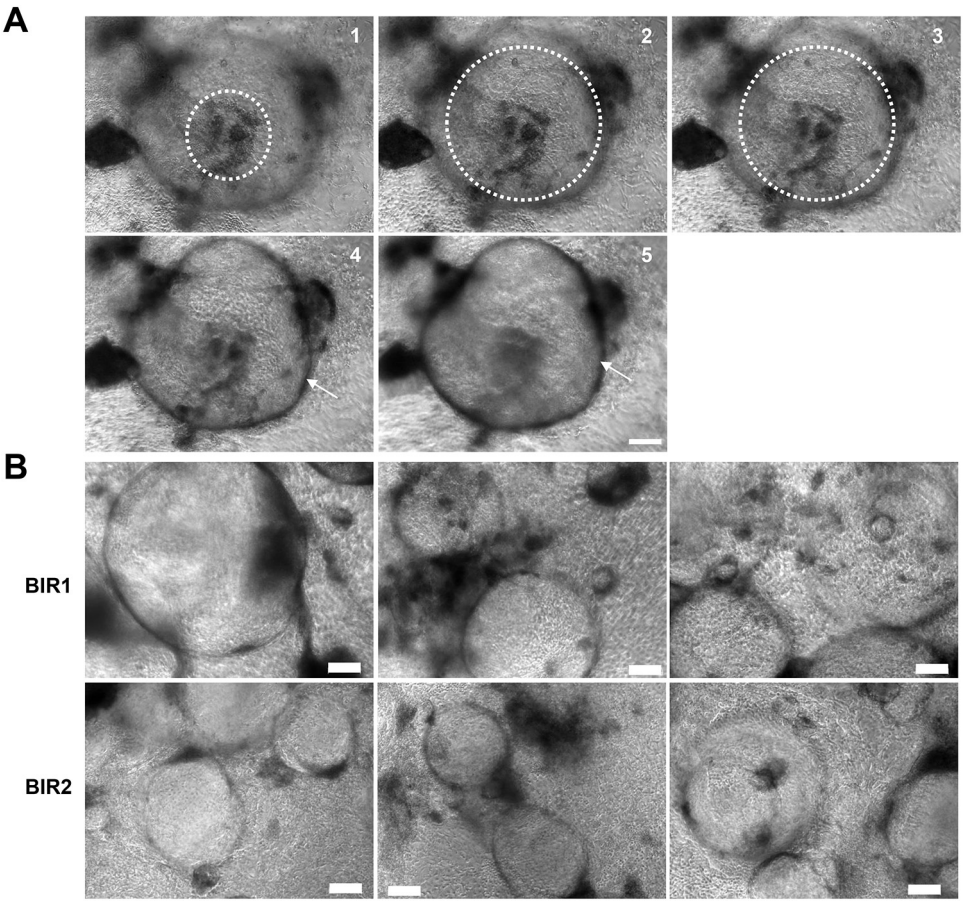

Fig. 2. Representative images of balloon structures. (A) A series of z-stack phase contrast images showing the bottom to the top (1 to 5) of a balloon. 1, white dashed circle: stalk; 2 and 3, white dashed circles: connection between the tip of the stalk and the bottom of the spherical structure; 4 and 5, white arrows: wall of the spherical structure. Scale bar: 200 μm. (B) Phase contrast images of balloon structures formed in BIR1 (top row) and BIR2 (bottom row) treated samples from 3 independent experiments. Scale bars: 200 μm.

in diameter (Fig. 2B). The suspended part of a balloon could move by following the flow of the culture medium while remaining linked to the culture surface by its stalk (Supplementary Video). Cells of mesenchymal morphology were sometimes seen attached to the outside of a balloon, either on the surface of the spherical structure or the stalk, such as those attached to the balloon in Supplementary Video. Balloon structures were never observed in DMSO control samples or in samples treated by any other compounds screened.

2.2. Structure-activity relationship (SAR) analysis reveals a structural module related to the activity of BIRs

A compound structurally similar to the BIRs, compound 5373490 (Fig. 3A; ChemBridge), was purchased and assayed in parallel with BIR1 and BIR2 in a

http://dx.doi.org/10.1016/j.heliyon.2016.e00133

Fig. 3. Structure-activity relationship (SAR) analysis identified a structural module related to BIR activity. (A) Chemical structure of 5373490. (B) Phase contrast images of H1 hESCs treated with DMSO, BIR1 (1 μM), BIR2 (1 μM), and 5373490 (1 μM and 5 μM) for 2 days under feeder-independent pluripotent culture condition (Methods and Materials), showing differences in colony morphologies. Scale bar: 100 μm. (C) Western blotting of OCT4 in H1 hESCs treated with DMSO and BIR1 (1 μM) for 2 days. α-TUBULIN was used as a loading control. An un-cropped image is shown in Supplementary Figure 1A. (D) Western blotting of OCT4 in H1 hESCs treated with DMSO and BIR2 (1 μM) for 2 days. α-TUBULIN was used as a loading control. An un-cropped image is shown in Supplementary Figure 1B. (E) Western blotting of OCT4 in H1 hESCs treated with DMSO and 5373490 (1 μM and 5 μM) for 4 days. α-TUBULIN was used as a loading control. An un-cropped image is shown in Supplementary Figure 1C.

http://dx.doi.org/10.1016/j.heliyon.2016.e00133

structure-activity relationship (SAR) analysis. Compared to BIR1 (Fig. 1B), BIR2 is missing a 2-hydroxylbenzyl group and two methyl groups at opposite ends of its structure (Fig. 1B). In 5373490, the 2-hydroxylbenzyl group is intact compared to BIR1 (Fig. 3A); however, the 2-(isobutylthio)benzo[*d*]thiazole group in BIR1 is replaced by a benzo[*d*]thiazol-2(3*H*)-one group (Fig. 3A).

Because BIR1 and BIR2 were originally identified from a high-throughput chemical screen [21] for their abilities at disrupting hESC pluripotency, we assayed the three compounds in parallel in hESCs maintained under feeder-free pluripotency culture condition (Methods and Materials) for their potencies at inducing hESC differentiation. As pluripotent hESCs typically grow in tightly packed colonies, loss of colony integrities caused by spreading of cells is commonly used as an indicator of differentiation [23, 24]. At a final concentration of 1 μM, both BIR1 and BIR2 efficiently induced spreading of cells and loss of colony integrities after 2 days of treatment (Fig. 3B); meanwhile both 1 μM and 5 μM 5373490 treatments failed to alter colony morphology, as compared to the DMSO control (Fig. 3B). We then examined the protein level of the key pluripotency factor OCT4 [19] under SAR compound treatments. 1 μM of BIR1 (Fig. 3C and Supplementary Figure 1A) and BIR2 (Fig. 3D and Supplementary Figure 1B) were both sufficient to significantly reduce OCT4 expression after 2 days of treatment; on the other hand, neither 1 μM nor 5 μM treatments of 5373490 affected OCT4 expression after 4 days (Fig. 3E and Supplementary Figure 1C). Last but not least, when applied under balloon-inducing condition, 5 μM 5373490-treated cells never gave rise to the formation of balloon structures.

Taken together, these results suggest that the 2-hydroxylbenzyl group present in BIR1 may be dispensable for the activities tested, whereas the structural integrity of the benzo[*d*]thiazole group and its attached functional group, such as the 2-methylpropane-1-thiol group in BIR1 and the ethanethiol group in BIR2 (Fig. 1B), may be required for the compounds' activities.

2.3. Gene expression profiling and functional assays revealed an endothelial identity of the balloons

Due to the apparent morphological similarities, we hypothesized an endothelial identity for the balloons, and examined this hypothesis using gene expression analyses and functional tests. Quantitative-PCR (qPCR) analysis showed elevated expressions of endothelial lineage-specific markers *VE-cadherin*, *KDR* (*VEGFR2*), *TIE1*, *TIE2*, *Endoglin*, and *FLT1* in balloon cultures as compared to the DMSO control (Fig. 4A). In contrast, the expression of mural cell (including vascular smooth muscle cells and pericytes) [25] marker *Calponin1* was not elevated (Fig. 4A). Fluorescent-activated cell sorting (FACS) analysis also showed that the expressions of endothelial markers VE-cadherin, CD31, CD34, KDR, CXCR4, and

http://dx.doi.org/10.1016/j.heliyon.2016.e00133

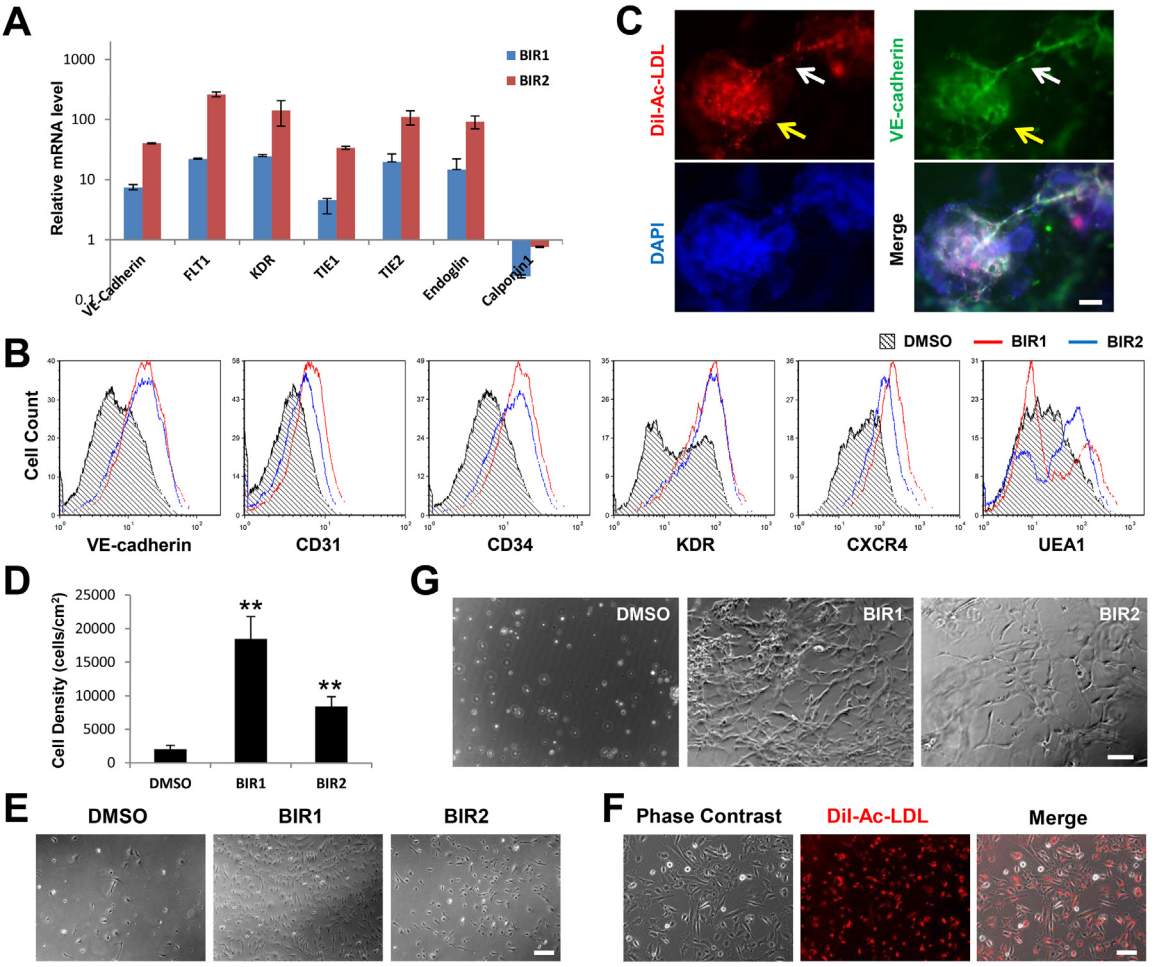

Fig. 4. Gene expression analyses and functional tests revealed an endothelial identity of the balloons. (A) Quantitative-PCR analysis of endothelial markers and the mural cell-specific marker *Calponin1* in H9 hESCs treated with DMSO, BIR1 (5 μM), and BIR2 (5 μM), and cultured till day 12. All values were normalized to the level (=1) of mRNA in DMSO treated cells. Each bar represents mean ± SD (error bars). *ACTB* (β-*actin*) was used as a loading control. n = 3 independent experiments. (B) FACS analysis of VE-cadherin, CD31, CD34, KDR, CXCR4, and UEA1 in H9 hESCs treated with DMSO, BIR1, and BIR2, and cultured till day 12. n > 3 independent experiments. (C) Fluorescent images of a balloon stained with DiI-Ac-LDL (red), VE-cadherin (green), and DAPI (blue), showing a balloon fallen on its side. Yellow arrows: spherical structure; white arrows: stalk. Scale bar: 200 μm. (D) Quantification of fibronectin selective adhesion assay. H9 hESCs were treated with DMSO, BIR1, and BIR2 for 6 days, let grown till day 12, and re-plated onto fibronectin coated plates and maintained in endothelial culture medium for 3 days. Cell densities were calculated from 3 independent experiments. Each bar represents mean ± SD (error bars). **: $p < 0.01$. (E) Phase contrast images of H9 hESCs treated by DMSO, BIR1 (5 μM), and BIR2 (5 μM) for 6 days, let grown till day 12, and then re-plated onto fibronectin coated plates and maintained in endothelial culture medium for 3 days. Scale bar: 200 μm. (F) Phase contrast (left), DiI-Ac-LDL fluorescent (middle), and merged (right) images of H9 hESCs treated by BIR1 (5 μM) for 6 days, cultured till day 12, and replated onto fibronectin coated plates and maintained in endothelial culture medium for 3 days. Scale bar: 100 μm. (G) Phase-contrast images of H9 hESCs treated with DMSO, BIR1, and BIR2, cultured till day 12, and then encapsulated by Matrigel and maintained in endothelial culture medium for 5 days. Scale bar: 200 μm.

http://dx.doi.org/10.1016/j.heliyon.2016.e00133

UEA1 (a human endothelial cell-specific lectin) [26] were elevated in balloon cultures as compared to the DMSO control (Fig. 4B). Furthermore, both spherical structures (Fig. 4C, yellow arrows) and stalks (Fig. 4C, white arrows) stained positive for VE-cadherin and DiI-Ac-LDL (Fig. 4C, a balloon fallen on its side is shown to demonstrate staining of the entire balloon structure). DiI-Ac-LDL, DiI-labeled Low Density Lipoprotein (LDL), binds to LDL receptors and thus specifically labels cells of endothelial identity [27] (Methods and Materials).

Functional Assays further confirmed an endothelial identity of the balloons. In a selective-adhesion assay (Methods and Materials), 12-day balloon cultures and DMSO controls were trypsinized and re-plated under an endothelial-selective culture condition at the same seeding density; significantly higher numbers of adherent cells were observed in wells seeded by balloon cultures (Fig. 4D and Fig. 4E). In all three treatment groups tested (DMSO, BIR1, and BIR2), nearly all adherent cells stained positive for DiI-Ac-LDL, verifying the endothelial-selectivity of this assay (Fig. 4F). Furthermore, when tested in a Matrigel vessel-formation assay (Methods and Materials), an assay commonly used to examine the ability of cells to form vascular networks *in vitro*, BIR-treated cells converted to an elongated morphology and actively assembled into vessel-like networks when encapsulated in Matrigel, whereas DMSO-treated cells never showed vessel-forming activity (Fig. 4G). Altogether, several independent lines of evidence suggested an endothelial identity of the balloons.

2.4. Cell surface marker analyses identified a VE-cadherin $^{+}$CD31^{+}CD34^{+}KDR^{+}CD43^{-} putative endothelial progenitor population

Because balloons were able to emerge *de novo* and subsequently grow in size, we hypothesize that an endothelial progenitor population may be present in the balloon cultures and responsible for balloon morphogenesis. To test this hypothesis, we examined the surface marker expression profile of individual cells in the balloon cultures using FACS analysis. Because immunostaining revealed a DiI-Ac-LDL^{+}VE-cadherin^{+} expression profile for balloons (Fig. 4C), and because VE-cadherin is known as a key molecular marker of endothelial progenitors [28], we first examined the overall percentage of VE-cadherin^{+} cells in balloon cultures. FACS analyses revealed a distinct VE-cadherin^{+} population which constituted approximately 0.1–0.8% of the total cell population of a 12- to 13-day balloon culture (Fig. 5A, top-left plot, blue gate). Furthermore, nearly all VE-cadherin^{+} cells positively expressed endothelial progenitor markers KDR and CD31 (Fig. 5A, top row, blue gate and arrows). When plotted against the side scatter channel (SSC), CD31^{+} cells also appeared as a distinct population (Fig. 5A, bottom row, blue arrow and green gate); this population was also nearly exclusively VE-cadherin^{+} (Fig. 5A, bottom row, green gate and arrows), indicating the existence of a VE-cadherin^{+}CD31^{+}

http://dx.doi.org/10.1016/j.heliyon.2016.e00133

http://dx.doi.org/10.1016/j.heliyon.2016.e00133

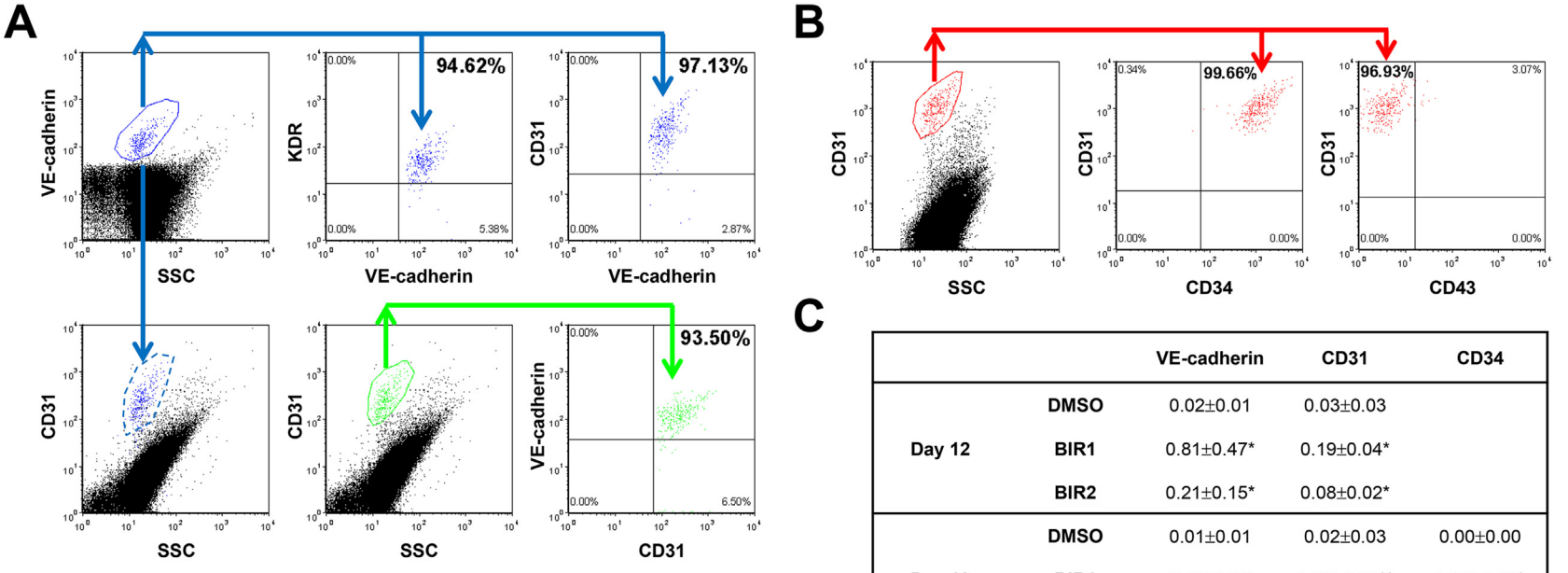

C

		VE-cadherin	CD31	CD34
Day 12	DMSO	0.02±0.01	0.03±0.03	
	BIR1	0.81±0.47*	0.19±0.04*	
	BIR2	0.21±0.15*	0.08±0.02*	
Day 13	DMSO	0.01±0.01	0.02±0.03	0.00±0.00
	BIR1	0.12±0.07	0.53±0.12**	0.30±0.12*
	BIR2	0.07±0.06	0.32±0.13*	0.18±0.11

Fig. 5. Identification of a VE-cadherin$^+$CD31$^+$CD34$^+$KDR$^+$CD43$^-$ population. (A) FACS analysis of VE-cadherin, CD31, and KDR in H9 hESCs treated with BIR1 (5 μM) and cultured for 13 days, showing a distinct VE-cadherin$^+$CD31$^+$KDR$^+$ population by gating VE-cadherin (top panel). CD31$^+$ cells also appear as a distinct population and is also VE-cadherin$^+$ (bottom panel). Quadrant gates were set up using DMSO control. n = 3 independent experiments. (B) FACS analysis of CD31, CD34, and CD43 in H9 hESCs treated with BIR1 (5 μM) and cultured for 12 days, showing a distinct CD31$^+$CD34$^+$CD43$^-$ population. Quadrant gates were set up using DMSO control. n = 3 independent experiments. (C) Quantifications of the percentages of VE-cadherin$^+$, CD31$^+$, and CD34$^+$ populations on days 12 and 13 in H9 hESCs treated with DMSO, BIR1, and BIR2. Each data point represents mean ± SD. *: $p < 0.05$, **: $p < 0.01$. n = 3 independent experiments.

population in balloon cultures. Because CD31 is also a marker of the hematopoietic lineage [29], to further verify the endothelial identity of the $CD31^+$ population, we triple stained cells with CD31, endothelial and hematopoietic progenitor marker CD34 [30], and hematopoietic lineage-specific marker CD43 [31]. As a result, $CD31^+$ cells were predominantly $CD34^+$, but $CD43^-$ (Fig. 5B), thus demonstrating an endothelial rather than hematopoietic identity of this population.

Taken together, these results suggested that a population of VE-$cadherin^+CD31^+CD34^+KDR^+CD43^-$ cells, a potential endothelial progenitor population judging by its surface marker expression profile, was present in balloon cultures and may be responsible for balloon formation. Quantifications of the population-level expressions of VE-cadherin, CD31, and CD34 at days 12 and 13 are summarized in Fig. 5C. BIR1 treatments produced higher percentages of VE-$cadherin^+$, $CD31^+$, and $CD34^+$ populations on both days 12 and 13 as compared to BIR2 (Fig. 5C). The presence of these populations in DMSO controls was minimum (Fig. 5C).

2.5. Morphological examination of a typical balloon culture revealed distinct DiI-Ac-LDL^+ multi-cellular modules

To better understand the balloon formation process, we conducted a more thorough morphological examination of the balloon cultures, focusing on the time of balloon formation (days 12 – 13). The general appearances of balloon cultures between days 12–13 were highly heterogeneous; balloons continued to emerge during this period of time, thus in theory structures representing various stages of balloon formation should be present in the same culture. To distinguish endothelial structures from the rest of the culture, we incubated live cultures with DiI-Ac-LDL before microscopic examination.

Several distinct multi-cellular modules formed by DiI-Ac-LDL^+ cells were identified. First, while cells in most areas of a balloon culture were spread out and appeared mesenchymal in morphology, some areas of the culture maintained an epithelial appearance; within these areas, clusters of DiI-Ac-LDL^+ cells with mesenchymal characteristics were found (Fig. 6, first column on the left) and will be hereafter referred to as “clusters”. Second, distinct DiI-Ac-LDL^+ cell aggregates with no apparent internal structural organizations were frequently observed (Fig. 6, second column) and will be referred to as “aggregates” hereafter. We were unable to determine if the aggregates were uniformly solid in nature without any hidden internal structural organization based on the DiI-Ac-LDL staining result alone. Third, some spherical structures were found to remain directly attached to the culture surface (without “stalks” and could not move); they were smaller in sizes compared to the spherical structures in suspended balloons (Fig. 6, third column), and will be referred to as “spheres” hereafter. And finally, balloons were stained positive for DiI-Ac-LDL (Fig. 6, fourth column) as expected.

http://dx.doi.org/10.1016/j.heliyon.2016.e00133

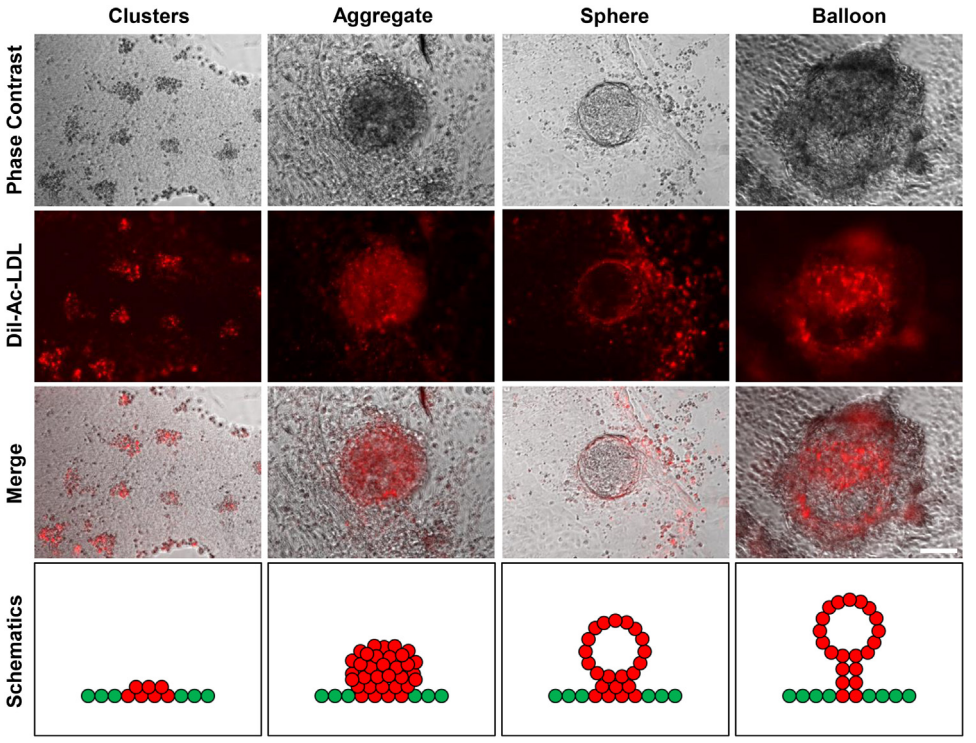

Fig. 6. Morphological analysis of a typical balloon culture revealed distinct DiI-Ac-LDL$^+$ multi-cellular modules. Top three rows: phase contrast, fluorescent, and merged images of H9 hESCs treated with BIR2 (5 μM) and cultured for 13 days, showing DiI-Ac-LDL$^+$ clusters (left), an aggregate (middle left), a sphere (middle right), and a balloon (right). Bottom row: schematic drawings of each structure. Filled green circles: DiI-Ac-LDL$^-$ cells; filled red circles: DiI-Ac-LDL$^+$ cells. Scale bar: 100 μm.

2.6. Further molecular marker analyses of the DiI-Ac-LDL$^+$ modules shed light on the identity of cluster cells and uncovered a VEGFR3$^+$ sprouting structure in aggregates

Based on these morphological observations we propose a working model of balloon formation (Fig. 7A) by hypothesizing that the DiI-Ac-LDL$^+$ multi-cellular modules represent intermediate structures of balloon-formation. We propose that clusters may represent an early progenitor population responsible for the initiation of balloon formation; clusters grow to form aggregates, which then self-organize into hollow spheres; spheres eventually develop stalk structures which allow them to elevate above the culture surface to form balloons. Although we were unable to acquire direct evidences such as time-lapse imaging to demonstrate this hypothesized transition between the DiI-Ac-LDL$^+$ modules during balloon-formation and thus conclusively verify our theory, we have nevertheless attempted to partially demonstrate the feasibility of our working model by further investigating cellular and molecular characteristics of the DiI-Ac-LDL$^+$ modules.

http://dx.doi.org/10.1016/j.heliyon.2016.e00133

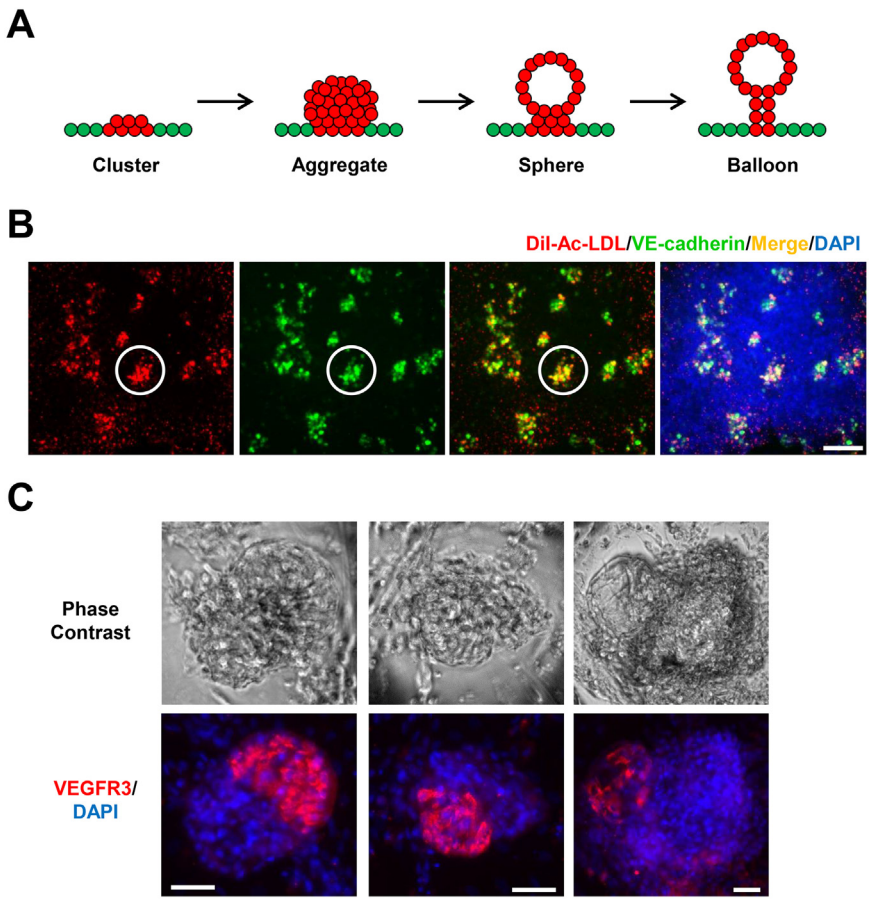

Fig. 7. Molecular marker analyses of the DiI-Ac-LDL$^+$ modules shed light on the identity of cluster cells and revealed a VEGFR3$^+$ sprout-like structure in aggregates. (A) Schematic drawings of a working model of balloon formation. (B) Fluorescent images of DiI-Ac-LDL (red), VE-cadherin (green), merged (yellow), and DAPI (blue) in H9 hESCs treated with BIR2 (5 μM) and cultured for 13 days, showing DiI-Ac-LDL$^+$VE-cadherin$^+$ clusters (white circle). Scale bar: 100 μm. (C) Phase contrast and immunofluorescent staining images of VEGFR3 (red), showing 3 sprout-like structures in cell aggregates (left, middle, and right columns) formed in a H9 hESC culture treated with BIR2 (5 μM). Scale bars: 50 μm.

First, to demonstrate that clusters may represent an early progenitor population, we performed double-staining of DiI-Ac-LDL and VE-cadherin, and showed that a majority of the cells within the clusters were indeed DiI-Ac-LDL$^+$VE-cadherin$^+$ (Fig. 7B; a distinct cluster is enclosed by a white circle), with VE-cadherin being a key endothelial progenitor marker [28]. However, the direct contribution of clusters to the formation of other DiI-Ac-LDL$^+$ modules cannot be determined by this result alone.

Second, to show that aggregates can indeed self-organize into hollow sphere structures, we attempted to search for evidences of the existence of a vascular

http://dx.doi.org/10.1016/j.heliyon.2016.e00133

sprouting event by examining the expression of VEGFR3, a marker highly expressed in angiogenic sprouts during embryonic vascular morphogenesis [32, 33], in aggregates. We found that within a subgroup of the seemingly structure-less cell aggregates, a subset of the cells was positively stained for VEGFR3 and spontaneously organized into sprout-like structures (Fig. 7C), once again supporting our proposed model (Fig. 7A).

3. Discussion

In this study, we conducted a chemical screen designed based on a novel hypothesized approach of hESC organoid induction, and successfully identified small molecules BIR1 and BIR2 as inducers of a self-organizing 3-D structure that was demonstrated to be of an endothelial identity. Free of growth-factor guidance, this method provided a novel hESC 3-D self-organization culture system based solely on small molecule induction. However, although this study intended to discover novel small molecule inducers of organoids, a 3-D structure should only qualify as an organoid if it contains more than one cell type which are arranged in a way that bears significant resemblance to the micro-anatomy of a natural organ, and thus balloons are not complex enough to be called an organoid.

A simple structure-activity relationship (SAR) assay was performed. Only one SAR compound [5373490] was tested in parallel with BIRs due to the limited commercial availability of structurally related compounds. Results from this assay (Fig. 3B–E) tentatively suggested a correlation between the integrity of the benzo [*d*]thiazole group and its attached functional group such as the 2-methylpropane-1-thiol group in BIR1 and the ethanethiol group in BIR2 (Fig. 1B), and the activities of the compounds. It must be noted that due to the limited number of SAR compounds tested, this result is far from being conclusive and should only be considered as a preliminary clue for the future follow-up studies such as a more comprehensive SAR analysis. As for the potential difference in potencies between BIR1 and BIR2, although both compounds induced balloon formation to similar densities (Results; 1.2 ± 0.8 balloons/cm^2 for BIR1 and 1.1 ± 0.1 balloons/cm^2 for BIR2), the fact that quantification of the VE-cadherin$^+$, CD31$^+$, and CD34$^+$ populations showed that BIR1 gave rise to higher percentages of these populations in the time course examined (Fig. 5C), and that BIR1, but not BIR2, induced balloon formation at 2.5 μM concentration (Results), indicated that BIR1 may possess a marginally higher potency compared to BIR2.

Although it is tempting for the authors to claim potential use of this method for the generation of endothelial progenitors and, subsequently, for regenerative medicine purposes, the efficiency of this differentiation is too low (Fig. 5C; approximately 0.1–0.8% VE-cadherin$^+$, 0.1–0.5% CD31$^+$, and 0.2–0.3% CD34$^+$ cells at days 12 to 13) for us to confidently exert that claim. Therefore, this article focuses only on

http://dx.doi.org/10.1016/j.heliyon.2016.e00133

the establishment and demonstration of a small molecule-based 3-D self-organizing culture system – the balloon-formation system – from hESCs.

Upon close examination of this system using various techniques, and upon analyzing the cellular, molecular, and morphological data acquired, we formed a working hypothesis of balloon formation to reconcile our findings. In this model we propose that balloons arise from sequential formation and transformation of precursory and intermediate multi-cellular modules including clusters, aggregates, and spheres (Fig. 7A). Although unable to conclusively verify this progressive transformation model of balloon formation, we conducted experiments to partially test this hypothesis, and demonstrated that clusters likely represent an early progenitor population (Fig. 7B) and that a self-organizing event similar to vascular sprouting takes place in the seemingly structure-less aggregates and may be responsible for the formation of spheres (Fig. 7C). Further analyses such as time-lapse imaging are required to definitively prove our working hypothesis.

3-D hESC self-organizing culture systems offer a unique opportunity to study potential mechanisms of early human development *in vitro*. We believe that the system described in this report, constructed using a unique chemical biology approach, makes a valuable addition to the growing list of hESC self-organizing culture systems and may potentially facilitate the investigation of human embryonic organogenesis. In fact, by examining the process of balloon morphogenesis, we have discovered a putative early endothelial progenitor population with a surface marker expression profile of VE-cadherin^{+}CD31^{+}CD34^{+}KDR^{+}CD43^{-} which to our knowledge has not been reported prior to this study. More works are needed to thoroughly exploit the potential of this system; for example, the detailed cellular and molecular control of the formation of VEGFR3^{+} sprouts from the aggregates (Fig. 7C) certainly warrants further investigation. Finally, identification of the biological target of BIR1/2 is required to fully elucidate the molecular pathway responsible for the initiation of balloon self-organization.

4. Methods and materials

4.1. Cell culture

H9 and H1 hESC lines (WiCell Research Institute, Madison, WI) were maintained under a feeder condition or a feeder-independent condition. For the feeder condition [23], primary mouse embryonic fibroblasts (MEFs) prepared from embryos of pregnant CF-1 mice (day 13.5 of gestation; Charles River) were cultured in Dulbecco's Modified Eagle Medium (DMEM) containing 10% FBS (Hyclone), 1% non-essential amino acids (NEAA; Invitrogen), and penicillin/streptomycin, and mitotically inactivated by gamma irradiation. H9 and H1 hESCs were cultured on irradiated MEFs in media containing DMEM/F12, 20% knockout

http://dx.doi.org/10.1016/j.heliyon.2016.e00133

serum replacement (KSR; Invitrogen), 4 ng/ml basic fibroblast growth factor (bFGF; Invitrogen), 1% NEAA, 1 mM glutamine, and 0.1 mM β-mercaptoethanol. For the feeder-independent condition, hESCs were cultured on Matrigel (BD Biosciences)-coated plates in mTeSR1 medium (StemCell Technologies) as described [24]. Experiments described in this study were conducted with H9 and H1 hESCs between passages 30 and 60.

4.2. Morphological screen

For the morphological screen, H9 and H1 hESCs were plated in Matrigel coated vessels as 2-D cultures in a basal medium composed of RPMI-1640 medium and 2% B-27 supplement (Invitrogen). Differentiation-inducing small molecules identified from a previous large-scale chemical screening [21] were individually applied at 5 μM to each culture, and incubated for 6 days before withdrawn. Medium was changed every other day with compound replenishment. Cultures were then kept in the basal medium without the addition of growth factors, and let grown for 6 days or longer, with medium change every other day. During this prolonged incubation period, cultures were examined regularly under microscope for the emergence of 3-D organoid-like structures.

4.3. Balloon culture

90% confluent H9 and H1 hESC cultures maintained on MEF feeders or on Matrigel-coated vessels were dissociated by brief exposure to type IV collagenase (1 mg/ml; Invitrogen) or Dispase (Invitrogen), respectively, followed by mechanical dissociation into cell clumps. It is crucial to plate cells as clumps rather than as single cells to allow successful balloon formation. Cell clumps were seeded into Matrigel coated vessels in mTeSR1 medium at high density: generally at a 1:2 passaging ratio for MEF-cultured cells, and 1:1 for Matrigel-cultured cells. Cultures were then maintained in mTeSR1 medium with daily medium change until reaching approximately 90% confluency. The degree of confluency before compound induction must be carefully controlled, as both over- and under-confluency affect the efficiency of balloon formation. On day 0, culture medium was switched to a basal differentiation medium containing Advanced RPMI 1640 (Invitrogen), 2% B-27 supplement (Invitrogen), and 1% Glutamax (Invitrogen). Medium was changed every other day throughout the differentiation protocol. BIR1 and BIR2 were applied and replenished along with fresh basal differentiation medium at 5 μM from day 0 to day 6. Balloons typically emerge at days 12 to 13.

4.4. Western blotting

Cultured cells were lysed directly by 2 × Laemmli buffer (Bio-Rad), boiled for 5 min, and analyzed using SDS-PAGE electrophoresis followed by wet-transfer

http://dx.doi.org/10.1016/j.heliyon.2016.e00133

onto nitrocellulose membranes using a system manufactured by Bio-Rad. The membranes were blocked using blocking solution (5% BSA in Tris-buffered saline containing 0.1% Tween-20 [TBST]), and then incubated with TBST-diluted primary antibodies (Table 1) at 4 °C overnight. The membranes were then washed by TBST for 3 × 5 min, and incubated with horse radish peroxidase (HRP) conjugated secondary antibodies at room temperature for 1 h. Finally, the membranes were washed 3–5 × 5 min by TBST and developed using Super-Signal West Pico Chemiluminescent Substrate (Pierce).

4.5. RNA extraction, reverse transcription, and quantitative-PCR

Total RNA were isolated using RNeasy mini kit (QIAGEN). cDNAs were synthesized from the purified RNAs using Reverse Transcription System (Promega). Quantitative-PCR was performed using QuantiTech SYBR Green PCR kit (QIAGEN). Signals were analyzed using the comparative C_T method, and *ACTB* gene was used as an internal control. Primer sequences are listed in Table 2.

Table 1. Antibodies and fluorescent dyes.

Antibody	Source	Catalog Number	Dilution
OCT4	Santa Cruz	sc-9081	1:1,000 (WB)
α-TUBULIN	Abcam	ab11304	1:10,000 (WB)
VE-cadherin	R&D Systems	AF938	1:500 (IF)/1:50 (FACS)
VEGFR3	Millipore	MAB3757	1:50 (IF)/1:50 (FACS)
CD31-PE	BD Biosciences	560983	1:5 (FACS)
CD31-FITC	BD Biosciences	555445	1:5 (FACS)
VE-cadherin-Alexa647	BD Biosciences	561567	1:20 (FACS)
KDR-PE	BD Biosciences	560494	1:5 (FACS)
CD34-APC	BD Biosciences	560940	1:5 (FACS)
CD43-FITC	BD Biosciences	560978	1:5 (FACS)
CXCR4	R&D Systems	MAB172	1:1000 (FACS)
CD34	Millipore	CBL496	1:50 (FACS)
KDR	Millipore	05-554	1:50 (FACS)
Donkey anti-mouse, Alexa 488	Invitrogen	A-21202	1:200 (FACS)
Donkey anti-goat, Alexa 488	Invitrogen	A-11055	1:200 (FACS/IF)
Donkey anti-mouse, Alexa 594	Invitrogen	A-21203	1:200 (FACS/IF)
UEA1-Fluorescein	Vector Labs	FL-1061	1:1000 (FACS)
DiI-Ac-LDL	Biomedical Technologies	BT-902	1:20 (IF)

(WB: Western blotting; IF: immunofluorescence).

http://dx.doi.org/10.1016/j.heliyon.2016.e00133

4.6. Flow cytometry

Single cell suspensions were acquired through Accutase (Invitrogen) treatment. Cells were stained using conjugated or unconjugated antibodies or UEA1 lectin (Table 1) for 30 min on ice. Cells stained by unconjugated antibodies were washed by ice cold FACS buffer (PBS supplemented with 1% BSA) and then stained using fluorescent-conjugated secondary antibodies (Table 1) for an extra 30 min. Cells were then washed and resuspended in ice cold FACS buffer and analyzed using a BD Biosciences LSR II flow cytometry analyzer and BD FACSDiva software.

4.7. Immunofluorescent staining

Cells were washed once with phosphate-buffered saline (PBS) and fixed by 4% paraformaldahyde (Santa Cruz) at room temperature for 15 min and then blocked with 5% donkey serum (Sigma) in PBS at room temperature for 1 h. The samples were incubated with primary antibodies in PBST (PBS supplemented with 1% Triton) at 4 °C overnight, washed three times by PBS, and then incubated with fluorescent-labeled secondary antibodies in PBST at room temperature for 1 h. Finally, cells were incubated with DAPI for 5 min, washed three times by PBS, and subjected to fluorescent microscopy analysis (Zeiss).

4.8. Selective adhesion assay

Cells from balloon cultures and DMSO control were trypsinized into single cells, counted using a hematocytometer, and seeded into Fibronectin (BD Biosciences) coated culture vessels in endothelial culture medium (ATCC) at a density of 1.5×10^4 cells/cm^2. Numbers of adherent cells and their endothelial identities were examined 3 days after seeding.

Table 2. qPCR primer sequences.

Primer Name	Forward Primer (5'-3')	Reverse Primer (5'-3')
ACTB	agagctacgagctgcctgac	cgtggatgccacaggact
VE-cadherin	gttcacgcatcggttgttcaa	cgcttccaccacgatctcata
FLT1	gtcacagaagaggatgaaggtgtc	cacagtccggcacgtaggtgatt
KDR	tttttgcccttgttctgtcc	tcattgttcccagcatttca
TIE1	agaacctagcctccaagatt	actgtagttcagggactcaa
TIE2	tccaaggatgtctctgctctc	ttggggtcatcctcggtat
Endoglin	ttcctggagttcccaacg	aggtgccattttgcttgg
Calponin1	ctgtcagccgaggttaagaac	gaggccgtccatgaagttgtt

http://dx.doi.org/10.1016/j.heliyon.2016.e00133

4.9. Matrigel assay

Cells from balloon cultures and DMSO control were trypsinized into single cells, counted using a hematocytometer, and encapsulated in Matrigel (kept cool to prevent gelation) at 1.0×10^6 cells/ml. Cultures were then kept in 37 °C for 1 h to allow formation of solid gels. Endothelial culture medium (ATCC) was added to each well. Medium was changed every other day. The emergences of vessel-like networks were monitored, and images were acquired using microscopy (Zeiss).

4.10. DiI-Ac-LDL staining

DiI-Ac-LDL were added to live cell culture at a 1:20 dilution and incubated at 37 °C for 4 h. Medium was then removed, and cells were washed with cell culture medium and visualized via fluorescent microscopy (Zeiss).

4.11. Statistical analysis

Statistical analyses were performed using Microsoft Excel. Student's t-test was used to compare two experimental groups, assuming unequal variances. Differences are considered significant when $p < 0.05$.

Declarations

Author contribution statement

Bradley Feng: Performed the experiments.

Yijie Geng: Conceived and designed the experiments; Performed the experiments; Analyzed and interpreted the data; Wrote the paper.

Funding statement

This work was supported by the National Institutes of Health (NIH) (GM083812) and NSF Science and Technology Center Emergent Behaviors of Integrated Cellular Systems (EBICS) (CBET-0939511).

Competing interest statement

The authors declare no conflict of interest.

Additional information

Supplementary content related to this article has been published online at http://dx.doi.org/10.1016/j.heliyon.2016.e00133

Acknowledgments

We thank Dr. Hyunjoon Kong and Dr. Nihan Yonet-Tanyeri for valuable scientific discussion.

References

[1] M. Eiraku, N. Takata, H. Ishibashi, M. Kawada, E. Sakakura, S. Okuda, et al., Self-organizing optic-cup morphogenesis in three-dimensional culture, Nature 472 (2011) 51–56.

[2] M. Eiraku, K. Watanabe, M. Matsuo-Takasaki, M. Kawada, S. Yonemura, M. Matsumura, et al., Self-organized formation of polarized cortical tissues from ESCs and its active manipulation by extrinsic signals, Cell Stem Cell 3 (2008) 519–532.

[3] T. Nakano, S. Ando, N. Takata, M. Kawada, K. Muguruma, K. Sekiguchi, et al., Self-formation of optic cups and storable stratified neural retina from human ESCs, Cell Stem Cell 10 (2012) 771–785.

[4] K. Muguruma, A. Nishiyama, Y. Ono, H. Miyawaki, E. Mizuhara, S. Hori, et al., Ontogeny-recapitulating generation and tissue integration of ES cell-derived Purkinje cells, Nat. Neurosci. 13 (2010) 1171–1180.

[5] H. Suga, T. Kadoshima, M. Minaguchi, M. Ohgushi, M. Soen, T. Nakano, et al., Self-formation of functional adenohypophysis in three-dimensional culture, Nature 480 (2011) 57–62.

[6] Y. Sasai, Next-generation regenerative medicine: organogenesis from stem cells in 3D culture, Cell Stem Cell 12 (2013) 520–530.

[7] F. Antonica, D.F. Kasprzyk, R. Opitz, M. Iacovino, X.H. Liao, A.M. Dumitrescu, et al., Generation of functional thyroid from embryonic stem cells, Nature 491 (2012) 66–71.

[8] L. Cao, J.D. Gibson, S. Miyamoto, V. Sail, R. Verma, D.W. Rosenberg, et al., Intestinal lineage commitment of embryonic stem cells, Differentiation 81 (2011) 1–10.

[9] H. Saito, M. Takeuchi, K. Chida, A. Miyajima, Generation of glucose-responsive functional islets with a three-dimensional structure from mouse fetal pancreatic cells and iPS cells in vitro, Plos One 6 (2011) e28209.

[10] T. Ueda, T. Yamada, D. Hokuto, F. Koyama, S. Kasuda, H. Kanehiro, et al., Generation of functional gut-like organ from mouse induced pluripotent stem cells, Biochem. Biophys. Res. Commun. 391 (2010) 38–42.

 http://dx.doi.org/10.1016/j.heliyon.2016.e00133

[11] X.L. Wang, K.M. Ye, Three-Dimensional Differentiation of Embryonic Stem Cells into Islet-like Insulin-Producing Clusters, Tissue Eng. Pt. A 15 (2009) 1941–1952.

[12] J. Mariani, M.V. Simonini, D. Palejev, L. Tomasini, G. Coppola, A.M. Szekely, et al., Modeling human cortical development in vitro using induced pluripotent stem cells, P. Natl. Acad. Sci. USA 109 (2012) 12770–12775.

[13] M.A. Lancaster, M. Renner, C.A. Martin, D. Wenzel, L.S. Bicknell, M.E. Hurles, et al., Cerebral organoids model human brain development and microcephaly, Nature 501 (2013) 373–379.

[14] Y. Xia, E. Nivet, I. Sancho-Martinez, T. Gallegos, K. Suzuki, D. Okamura, et al., Directed differentiation of human pluripotent cells to ureteric bud kidney progenitor-like cells, Nat. Cell Biol. 15 (2013) 1507–1515.

[15] J.R. Spence, C.N. Mayhew, S.A. Rankin, M.F. Kuhar, J.E. Vallance, K. Tolle, et al., Directed differentiation of human pluripotent stem cells into intestinal tissue in vitro, Nature 470 (2011) 105–109.

[16] K.W. McCracken, E.M. Cata, C.M. Crawford, K.L. Sinagoga, M. Schumacher, B.E. Rockich, et al., Modelling human development and disease in pluripotent stem-cell-derived gastric organoids, Nature 516 (2014) 400–404.

[17] J.M. Wells, J.R. Spence, How to make an intestine, Development 141 (2014) 752–760.

[18] M. Takasato, P.X. Er, M. Becroft, J.M. Vanslambrouck, E.G. Stanley, A.G. Elefanty, et al., Directing human embryonic stem cell differentiation towards a renal lineage generates a self-organizing kidney, Nat. Cell Biol. 16 (2014) 118–126.

[19] L.A. Boyer, T.I. Lee, M.F. Cole, S.E. Johnstone, S.S. Levine, J.P. Zucker, et al., Core transcriptional regulatory circuitry in human embryonic stem cells, Cell 122 (2005) 947–956.

[20] J. Shu, C. Wu, Y.T. Wu, Z.Y. Li, S.D. Shao, W.H. Zhao, et al., Induction of Pluripotency in Mouse Somatic Cells with Lineage Specifiers, Cell 153 (2013) 963–975.

[21] Y. Geng, Y. Zhao, L.C. Schuster, B. Feng, D.A. Lynn, K.M. Austin, et al., A Chemical Biology Study of Human Pluripotent Stem Cells Unveils HSPA8 as a Key Regulator of Pluripotency, Stem Cell Reports 5 (2015) 1143–1154.

 http://dx.doi.org/10.1016/j.heliyon.2016.e00133

[22] Y. Geng, B. Feng, Mesendogen, a novel inhibitor of TRPM6, promotes mesoderm and definitive endoderm differentiation of human embryonic stem cells through alteration of magnesium homeostasis, Heliyon 1 (2015) e00046.

[23] J.A. Thomson, J. Itskovitz-Eldor, S.S. Shapiro, M.A. Waknitz, J.J. Swiergiel, V.S. Marshall, et al., Embryonic stem cell lines derived from human blastocysts, Science (1998) 1145–1147.

[24] T.E. Ludwig, M.E. Levenstein, J.M. Jones, W.T. Berggren, E.R. Mitchen, J.L. Frane, et al., Derivation of human embryonic stem cells in defined conditions, Nat. Biotechnol. 24 (2006) 185–187.

[25] M. Sone, H. Itoh, K. Yamahara, J.K. Yamashita, T. Yurugi-Kobayashi, A. Nonoguchi, et al., Pathway for differentiation of human embryonic stem cells to vascular cell components and their potential for vascular regeneration, Arterioscl. Throm. Vas. 27 (2007) 2127–2134.

[26] L.K. Christenson, R.L. Stouffer, Isolation and culture of microvascular endothelial cells from the primate corpus luteum, Biol. Reprod. 55 (1996) 1397–1404.

[27] J.C. Voyta, D.P. Via, C.E. Butterfield, B.R. Zetter, Identification and Isolation of Endothelial-Cells Based on Their Increased Uptake of Acetylated-Low Density Lipoprotein, J. Cell Biol. 99 (1984) 2034–2040.

[28] D. Vestweber, VE-cadherin - The major endothelial adhesion molecule controlling cellular junctions and blood vessel formation, Arterioscl. Throm. Vas. 28 (2008) 223–232.

[29] C.I. Baumann, A.S. Bailey, W.M. Li, M.J. Ferkowicz, M.C. Yoder, W.H. Fleming, PECAM-1 is expressed on hematopoietic stem cells throughout ontogeny and identifies a population of erythroid progenitors, Blood 104 (2004) 1010–1016.

[30] Y. Nakajima-Takagi, M. Osawa, M. Oshima, H. Takagi, S. Miyagi, M. Endoh, et al., Role of SOX17 in hematopoietic development from human embryonic stem cells, Blood 121 (2013) 447–458.

[31] M.A. Vodyanik, J.A. Thomson, I.I. Slukvin, Leukosialin (CD43) defines hematopoietic progenitors in human embryonic stem cell differentiation cultures, Blood 108 (2006) 2095–2105.

[32] T. Tammela, G. Zarkada, E. Wallgard, A. Murtomaki, S. Suchting, M. Wirzenius, et al., Blocking VEGFR-3 suppresses angiogenic sprouting and vascular network formation, Nature 454 (2008) 656–660.

 http://dx.doi.org/10.1016/j.heliyon.2016.e00133

[33] R. Benedito, S.F. Rocha, M. Woeste, M. Zamykal, F. Radtke, O. Casanovas, et al., Notch-dependent VEGFR3 upregulation allows angiogenesis without VEGF-VEGFR2 signalling, Nature 484 (2012) 110–114.

http://dx.doi.org/10.1016/j.heliyon.2016.e00133